Shi *et al.*
Chinese Journal of Mechanical Engineering (2022) 35:72
https://doi.org/10.1186/s10033-022-00729-w

Chinese Journal of Mechanical Engineering

ORIGINAL ARTICLE

Open Access

A Fuzzy-based Sliding Mode Control Approach for Acceleration Slip Regulation of Battery Electric Vehicle

Qin Shi[1], Mingwei Wang[1], Zejia He[1], Cheng Yao[1], Yujiang Wei[1] and Lin He[2*]

Abstract

Due to quick response and large quantity of electric motor torque, the traction wheels of battery electric vehicle are easy to slip during the initial phase of starting. In this paper, a sliding mode control approach of acceleration slip regulation is designed to prevent the slip of the traction wheels. The wheel slip ratio is used as the state variable for the formulation of system dynamics model. The fuzzy algorithm is utilized to adjust the switch function of sliding mode controller. After stability and robustness analysis, the sliding mode control law is transferred into C code and downloaded into vehicle control unit, which is validated under wet and dry road conditions. The experimental results with a small overshoot and a quick response during starting indicate that the sliding mode controller has good control effect on the slip ratio regulation. This article proposes an acceleration slip regulation method that improves the safety during acceleration for battery electric vehicle.

Keywords: Electric motor torque, Wheel slip ratio, Stability, Fuzzy algorithm, Robustness analysis

1 Introduction

With the increasing attention of the environmental and energy issues, both reducing emissions of fuel vehicles and finding alternatives have become the first priority of the automotive industry currently. As a kind of zero-emission vehicles, battery electric vehicle (BEV) is gradually attracting more and more attention and becomes a research focus [1]. The acceleration slip regulation (ASR) system has been widely used in internal combustion engine (ICE) vehicles. Compared with the output torque of the ICE, the permanent magnet synchronous motor (PMSM) torque has the characteristics of quick-response and large-quantity, which makes wheel slip easily during the acceleration process [2], which not only reduces the driving efficiency of vehicle, accelerates tire wear, increase powertrain load and energy consumption, but also damage the driving maneuverability, stability and comfort. Therefore, the ASR is benefit to improve driving safety and reduce the risk of accidents for battery electric vehicle [3].

Measures of the anti-slip for ICE vehicles include cutting down the opening degree of throttles to reduce engine power, controlling wheel-side braking torque, and adjusting hold-down force of clutch [4]. Compared with the ICE, the PMSM has several advantages, such as rapid response and precise control [5]. Hence, the wheel slip can be controlled by regulating the output torque of electric motor [6].

Considering the security during the acceleration process, some literatures take the vehicle yaw moment into account. When the traction wheels are of slip, there will be a problem of generating undesired yaw moment and yaw angular velocity. For a battery electric vehicle with rear wheel drive alone, a dynamic torque distribution controller is designed to solve this problem [7]. On the basis of model predictive control (MPC), apart from the regulation of wheel slip, Yuan et al. optimized vehicle

*Correspondence: helin@hfut.edu.cn

[2] Laboratory of Automotive Intelligence and Electrification, Hefei University of Technology, Hefei 230009, China
Full list of author information is available at the end of the article

safety, braking performance, driver comfort, and energy efficiency by adding some additional cost functions [8].

Most of anti-slip systems focus on two-wheel independent drive (2WID) or four-wheel independent drive (4WID) electric vehicles. In fact, due to the disadvantages of immature technology and high cost, wheel hub motor is rarely applied into vehicle architecture [9]. In addition, it is essential for 4WID electric vehicles to be equipped with additional speed sensors due to adopting the slip-ratio-based anti-slip system. Therefore, most of literatures is still in a simulation stage and does not carry out verification on road test. In this paper, the research object is a rear-drive logistics BEV, the speed of which can be obtained by front wheels so that the designed approach will be tested and verified in engineering practice.

In the past ten years, some algorithms have been applied into this field [10]. Owing to the advantages of PID control that it does not depend on the system model, as well as dealing with uncertain and complex problems, Guo et al. took it as the core control algorithm. At the same time, for the assumption of constant longitudinal force, a compensator is designed to offset the calculation error [11]. However, the individual PID control is not suitable for changing environment. Li and Qu applied fuzzy PID control to ASR system. The parameters of the controller are amended in real time to make it satisfy the adaptability of nonlinear and time-variant system [12]. Considering the advantages of good robustness, adaptability, and better fault tolerance [13], fuzzy control is another method to solve the problem. Yin et al. put forward a kind of ASR control system, which is designed by controlling the difference of actual angular acceleration and the threshold of angular acceleration. Compensating an adjusting torque on the basis of the expected one, the slip ratio can be controlled in an ideal range [14]. However, fuzzy control will lead to low control accuracy and poor dynamic quality, but it is suitable for the use in conjunction with other control algorithms. A rolling optimization strategy instead of a global one-time optimization is used in MPC algorithm, which can compensate uncertainty timely and has better dynamic performance [15–17]. Sekour and Hartani proposed a non-linear model prediction (NMP) direct torque control (DTC) algorithm [18]. In this paper, a fuzzy controller is used to generate weight factors online, which can guarantee a high response speed under the flexible loads.

Sliding mode control (SMC) is a kind of non-linear control method and has many advantages like fast response, insensitive to parameter changes and disturbances, etc [19, 20]. Therefore, SMC is applied into ASR system by many literatures [21–25]. However, it will lead to system oscillation without targeted measures [21, 22, 26]. In order to make the system have a good dynamic quality during the process, an approach with a positive control gain coefficient is adopted in Ref. [23]. However, due to the existence of the ground longitudinal force observer, the error of the observer may cause the system to be unstable. In order to reduce the system oscillation, Zhou et al. applied a special switching function, which makes the system have less speed when near the sliding surface [24]. Ricardo et al. proposed a continuous SMC algorithm and the sign function are replaced by continuous approximation [25]. Experimental results show good performance of the slip regulation and robustness to disturbances.

In order to solve the problem of wheel slip during the acceleration process of battery electric vehicle, a sliding mode control approach is designed in this paper. Considering the system oscillation, a regulator based on fuzzy algorithm is established to adjust the key parameters of the controller. The effectiveness of the proposed control law has been validated in a battery electric vehicle.

The rest of this paper is given as follows. Section 2 introduces the vehicle control problem. In Section 3, the sliding mode controller and a factor correction algorithm based on fuzzy control algorithm is described. The Lyapunov stability and robustness analysis of the control laws are in Section 4. The experimental results are analyzed in Section 5. Finally, some concluding remarks are shown in Section 6.

2 Problem Description

2.1 Vehicle Architecture

The architecture of the tested 4.5 t rear-drive logistics BEV is illustrated in Figure 1, in which a new type of motor direct drive axle is adopted. Compared with the conventional motor drive axle architecture, this drive train is more compact, which can reduce the vehicle's unloaded mass by about 20% and increase the transmission efficiency by 10%. An open differential is used in the drive axle, which allows the two wheels to have different speeds while outputting the same torque. The PMSM can

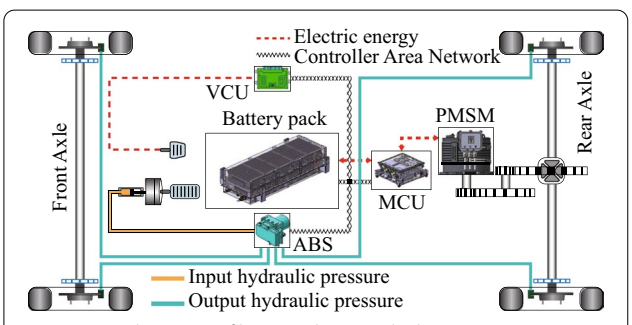

Figure 1 Architecture of battery electric vehicle

Table 1 Parameters of the on-board electric motor

Parameter	Value	Parameter	Value
Peak power (kW)	150	Rated power (kW)	70
Peak speed (r/min)	8600	Rated speed (r/min)	3290
Peak torque (N·m)	550	Rated torque (N·m)	203

output a peak torque in a short time and some parameters of the motor are shown in Table 1. The accelerator pedal is an electronic pedal with a voltage sensor in a range of 0.5−3.2 V to cover the entire pedal stroke. Anti-lock brake system (ABS) adopts wheel speed sensors to obtain angular speed in real-time. Controllers on board communicate with each other through controller area network (CAN).

The VCU obtains the maximum torque by estimating system capacity of the current state, which is mainly limited by the drive motor performance and the power. The torque T_{mot} limited by the motor depends on the external characteristic curve. The torque T_{bat} limited by the battery maximum discharge power can be obtained by the following formula,

$$P = \frac{Tn}{9550}, \tag{1}$$

where P is the maximum battery discharge power, kW; T is the motor torque, N·m; n is the motor rotation speed, r/min.

As mentioned above, the maximum torque T_{Cap} of the current state can be obtained by taking the smaller one between T_{mot} and T_{bat}. Besides, by applying lookup table method according to the pedal opening degree, the VCU can analyze driver's acceleration intention and the driver torque coefficient C_{Dri} can be gained. Finally, the execution torque T_{DCS} can be obtained as follows,

$$T_{\text{DCS}} = C_{\text{Dri}} \cdot \min(T_{\text{bat}}, T_{\text{mot}}) = C_{\text{Dri}} \cdot T_{\text{Cap}}. \tag{2}$$

2.2 Problem Discovery

There is a problem encountered in the development process of automobile. Due to the low-speed and high-torque working characteristics of PMSM, it is easy to cause wheels slip on the low-adhesion condition, which can lead to vehicle instability. Based on this problem, the following control objectives should be considered.

1) It must be reliable to prevent wheel from slipping during the traction process.
2) The vehicle can achieve good longitudinal acceleration performance on the premise of vehicle stability.
3) Practical application of the controller should be guaranteed.

As shown in Figure 2, when the slip ratio is in the optimal control zone, the biggest adhesion coefficient can be obtained. However, when a slip ratio is over the optimal value λ_{opt}, it will be difficult to achieve precise control and easy to cause a risk of side-slip. Therefore, at the same time, limiting the wheel slip ratio within the optimal control zone can ensure high longitudinal adhesion and avoid possible out-of-control. The relationship between the adhesion coefficient and the slip ratio can be expressed by the following formula [27, 28],

$$\mu_{\lambda i} = \frac{2\mu_{\max}\lambda_i\lambda_{\text{opt}}}{\lambda_i^2 + \lambda_{\text{opt}}^2}, \tag{3}$$

where $\mu_{\lambda i}$ is the wheel adhesion coefficient and λ_i is the wheel slip ratio. The selected Eq. (3) has high fitting accuracy both in the stable zone and the optimal control zone.

When the drive wheels exceed λ_{opt}, the ASR controller needs to be activated immediately. Therefore, a control approach is designed to solve the problem, which is when the VCU enters and exits ASR system.

2.3 Problem Solution

In this subsection, a brief description of the control approach is presented. As illustrated in Figure 3, the VCU is in the DCS by default. Before entering the ASR system, two judgments need to be performed.

Case 1: Due to the property of the slip ratio formula, the measurement errors of the wheel speed sensors are amplified when the vehicle drives in a low speed, which will cause a slip ratio mutation. Therefore, by setting a speed threshold v_{th}, the misjudging of the slip ratio can be eliminated.

Case 2: When $\lambda_{\max}$ is bigger than λ_{th}, the wheel is considered in a slippage state. With a view to the capacity limit, the smaller value between the ASR controller

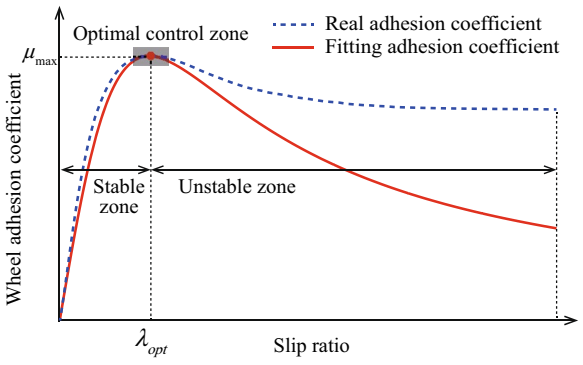

Figure 2 Relationship between adhesion coefficient and slip ratio

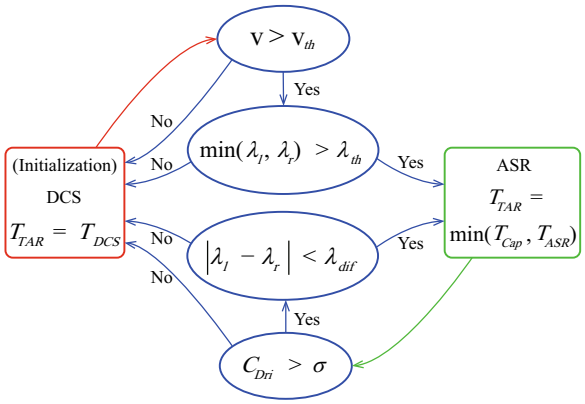

Figure 3 Traction torque control of acceleration slip regulation

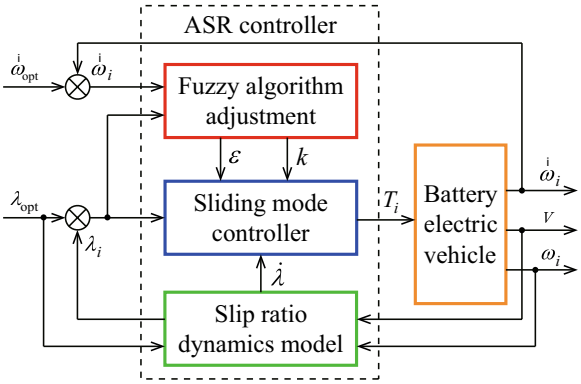

Figure 4 Architecture of sliding mode control approach

torque T_{ASR} and T_{CAP} is chosen as the final target torque T_{TAR}.

When the vehicle is in the ASR control mode, another two conditions will be judged in a loop.

Case 3: The driver's acceleration intention is estimated by comparing C_{Dri} with a threshold σ.

Case 4: The research in this paper focuses on the straight driving condition.

When the vehicle steers or the left and right adhesions are different, a slip difference between the two drive wheels will be generated. If Case 3 or Case 4 is not satisfied, the VCU will exit the ASR system immediately. Before entering another mode, it will always stay in the current state. During each judgment, anti-shake process is required and the time threshold is set as 10 cycles. The two control systems, DCS and ASR, can be switched in time according to the different working conditions, which makes the ASR system become a practical active safe driving assistance system.

3 Sliding Mode Controller

The structure of the ASR controller is shown in Figure 4, including the slip ratio dynamics model, sliding mode controller, and fuzzy algorithm adjustment.

3.1 Vehicle Dynamics

3.1.1 Slip Ratio Formulation

The wheel slip ratio is defined as follows,

$$\lambda = \frac{|v_\omega - v|}{\max(v_\omega, v)}, \tag{4}$$

where v_ω is the wheel linear speed, m/s; v is the vehicle longitudinal speed, m/s.

When the vehicle drives on the road with uneven adhesion coefficients, there will be a difference of slip ratio between the two drive wheels. Therefore, the "high-election principle" is adopted to take the larger slip ratio as the control object, before which, the larger wheel angular speed has to be obtained as follows,

$$\omega_i = \max(\omega_{\mathrm{l}}, \omega_{\mathrm{r}}), \tag{5}$$

where ω_{l} and ω_{r} are the angular speeds of the left and right wheels, respectively.

In the driving process, the relationship between v_ω and v satisfies $v_\omega \geq v$ all the time. Therefore, the larger slip ratio can be obtained as follows,

$$\lambda_i = \frac{v_\omega - v}{v_\omega} = \frac{r\omega_i - v}{r\omega_i}. \tag{6}$$

3.1.2 Wheel Dynamics Model

In this paper, the following points are assumed when the vehicle is simplified into a single wheel model.

1) The air resistance and wheel rolling resistance are ignored.
2) The left and right wheels have the same physical characteristics, such as the moment of inertia and rolling radius.

The formulation of wheel revolution can be obtained as follows,

$$J_i\dot{\omega}_i = T_i - rF_{xi}, \tag{7}$$

$$M\dot{v} = F_{xi}, \tag{8}$$

where J_i is the moment of inertia, kg·m^2; T_i is the driving torque on the wheel, N·m; r is the rolling radius of the wheel, m; F_{xi} is the wheel longitudinal force, N; and M is the half mass of the whole vehicle, kg.

The relationship between the ground longitudinal force F_{xi} and the ground normal force F_{zi} can be written as follows,

$$F_{xi} = \mu_{\lambda_i} F_{zi}. \tag{9}$$

3.1.3 Slip Ratio Dynamics

Because of the inherent discontinuous switching characteristics, in an actual system, there must be jitter near the sliding mode surface. Moreover, it is impossible to eliminate the jitter and it can only be weakened. For the ASR system applied to BEV, the high-frequency vibration generated by chattering will accelerate the wear of the transmission system, increase the load on the motor, and make the system unstable. In general, the chattering is caused by the following four parts.

1) The time lag of the switch.
2) The space lag of the switch.
3) The effect of system inertia.
4) Discrete system itself.

In short, when the system reaches the switching surface, the moving point passes through it due to the system inertia. Finally, chattering is formed and superimposes on the ideal sliding mode [29]. Therefore, the chattering can be weakened effectively by reducing the reaching speed and system inertia.

The derivative of Eq. (6) can be obtained as follows,

$$\dot{\lambda}_i = \frac{\dot{\omega}_i v - \omega_i \dot{v}}{r\omega_i^2}. \tag{10}$$

Substituting Eq. (7), Eq. (8), and Eq. (9) into Eq. (10), the differential equation of slip ratio is as follows,

$$\dot{\lambda}_i = \frac{vT_i}{J_i r\omega_i^2} - \mu_{\lambda i}\left(\frac{F_{zi} v}{J_i \omega_i^2} + \frac{F_{zi}}{rM\omega_i}\right). \tag{11}$$

Substituting Eq. (3) into Eq. (11), the slip ratio dynamics model is as follows,

$$\dot{\lambda}_i = \frac{vT_i}{J_i r\omega_i^2} - \frac{2\mu_{\max}\lambda_i\lambda_{\text{opt}}}{\lambda_i^2 + \lambda_{\text{opt}}^2}\left(\frac{F_{zi} v}{J_i \omega_i^2} + \frac{F_{zi}}{rM\omega_i}\right). \tag{12}$$

3.2 Control Law

The sliding mode surface is defined as follows,

$$S = \lambda_i - \lambda_{\text{opt}}. \tag{13}$$

In order to meet the arrival conditions while considering the approach speed and approach quality together, an improved exponential approach law is used in this paper as follows,

$$\dot{S} = -\varepsilon(S/\varphi\ )^2 \text{sgn}(S) - kS, \tag{14}$$

where φ is the thickness of the boundary layer, and sgn is the sign function.

Multiplying Eq. (13) by Eq. (14) to get the following formula,

$$S \cdot \dot{S} = -\frac{\varepsilon S^3 \text{sgn}(S)}{\varphi^2} - kS^2 < 0. \tag{15}$$

The approach law satisfies the existence conditions of the generalized sliding mode. Therefore, it satisfies the reachability condition of the sliding mode,

$$\dot{S} = \dot{\lambda}_i - \dot{\lambda}_{\text{opt}} = -\varepsilon(S/\varphi\ )^2 \text{sgn}(S) - kS. \tag{16}$$

Substituting Eq. (12) into Eq. (16) to obtain the sliding mode control law,

$$\begin{aligned} T_i = {} & \frac{2\mu_{\max}\lambda_{\text{opt}}\lambda_i}{\lambda_{\text{opt}}^2 + \lambda_i^2} r F_{zi} + \frac{2\mu_{\max}\lambda_{\text{opt}}\lambda_i}{\lambda_{\text{opt}}^2 + \lambda_i^2} \cdot \frac{J_i F_{zi}\omega_i}{Mv} \\ & - \frac{rJ_i\omega_i^2}{v}\left(\varepsilon(S/\varphi\ )^2 \text{sgn}(S) + kS\right). \end{aligned} \tag{17}$$

As can be seen from the formula above, the sliding mode control law consists of three parts. The first part $\frac{2\mu_{\max}\lambda_{\text{opt}}\lambda_i}{\lambda_{\text{opt}}^2+\lambda_i^2} r F_{zi}$ is the main part of the acceleration torque. The second part $\frac{2\mu_{\max}\lambda_{\text{opt}}\lambda_i}{\lambda_{\text{opt}}^2+\lambda_i^2} \cdot \frac{J_i F_{zi}\omega_i}{Mv}$ is the influence of the wheel inertia on the driving torque. The wheel moment of inertia is usually very small, which results in that this term has very little effect on the driving torque. The third part $\frac{rJ_i\omega_i^2}{v}\left(\varepsilon(S/\varphi\ )^2 \text{sgn}(S) + kS\right)$ is the control adjustment item. When the wheel slip ratio exceeds the threshold, this item will provide a negative torque to correct the total driving force, and vice-versa.

3.3 Fuzzy Algorithm

In this subsection, through a quantitative analysis of the relationship between the approach law coefficient (ALC) and chattering, an adaptive correction algorithm based on a fuzzy controller is proposed. When the error of the wheel angular acceleration and slip ratio is large, a larger ALC will be selected to achieve a faster approach speed and a smaller ALC will be selected when the error is small. The dynamical adjusting of the ALC can make the motion trajectory more suitable for the sliding mode surface, which can ensure the dynamic quality of the arrival process and reduce the high-frequency chattering of system at the same time.

Substituting Eq. (6) into Eq. (10),

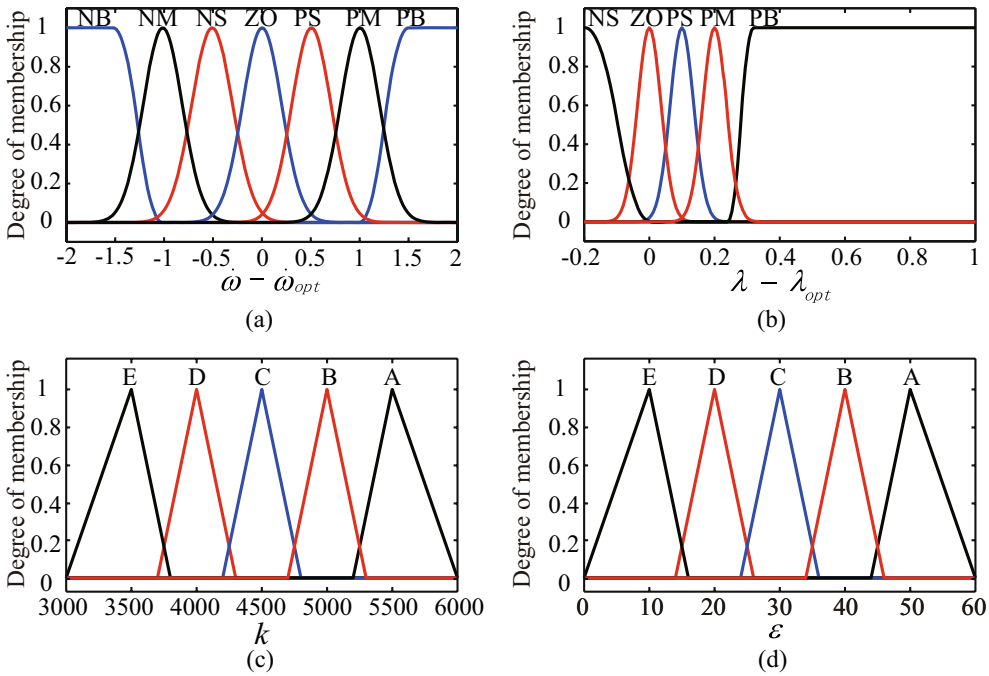

Figure 5 Membership function of Fuzzy algorithm variables

$$\dot{\lambda}_i = \frac{(1-\lambda_i)r\dot{\omega}_i - \dot{v}}{r\omega_i}. \tag{18}$$

When the wheel slip ratio is stable at a certain value, $\dot{\lambda}_i$ is 0, and the above formula becomes

$$\dot{\omega}_i = \frac{\dot{v}}{(1-\lambda_i)r}. \tag{19}$$

It can be seen from the equation above that when the slip ratio is stable, the wheel angular acceleration is correlated positively with the vehicle acceleration. Therefore, when the vehicle has the maximum acceleration, the optimal reference value of wheel angular acceleration can be obtained.

From Eq. (8) and Eq. (9), the maximum acceleration of a certain road is as follows,

$$\dot{v}_{\max} = \frac{F_{xi\max}}{M} = \frac{\mu_{\lambda_{\text{opt}}} F_{zi}}{M}. \tag{20}$$

Therefore, the reference optimal wheel angular acceleration is as follows,

$$\alpha_{\text{opt}} = \dot{\omega}_{\text{opt}} = \frac{\mu_{\lambda_{\text{opt}}} F_{zi}}{(1-\lambda_{\text{opt}})Mr}. \tag{21}$$

The first input variable is $\Delta E_1 = \lambda_i - \lambda_{\text{opt}}$. Based on the theoretical derivation and practical experience, in order to provide sufficient coverage, ΔE_1 is divided into five fuzzy subsets: [NS, ZO, PS, PM, PB]. The membership function is shown in Figure 5(a). 'N' and 'P' stand for 'Negative' and 'Positive', respectively. 'B', 'M', and 'S' stand for 'Big', 'Middle', and 'Small', respectively. The second input variable is $\Delta E_2 = \dot{\omega}_i - \dot{\omega}_{\text{opt}}$ and it is divided into seven fuzzy subsets: [NS, NM, NB, ZO, PS, PM, PB]. The membership function is shown in Figure 5(b).

In the fuzzy controller, the Mamdani method is used to perform the fuzzy logic calculation. The fuzzy rules are shown in Table 2. The defuzzification method is the gravity center. Based on the multiple simulation results, the factors are divided into five fuzzy subsets: [A, B, C, D, E], and the membership function is shown in Figure 5(c) and (d).

Table 2 Fuzzy rule

ε/k	NS	ZO	PS	PM	PB
NB	AA	BB	CC	DD	EE
NM	BB	CC	DD	EE	DD
NS	CC	DD	EE	DD	CC
ZO	DD	EE	DD	CC	BB
PS	EE	DD	CC	BB	BB
PM	DD	CC	BB	BB	AA
PB	CC	BB	BB	AA	AA

4 Controller Analysis

4.1 Stability Analysis

In order to verify the stability of the proposed closed-loop controller, the Lyapunov function is defined as the following,

$$V = \left(\lambda_i - \lambda_{\text{opt}}\right)^2. \tag{22}$$

It can be seen from Eq. (22) that the control system energy function is positive definite. To ensure the asymptotic stability of the system, the derivative of V should be negative definite and computed as follows,

$$\dot{V} = 2\left(\lambda_i - \lambda_{\text{opt}}\right). \tag{23}$$

Substituting Eq. (14) into Eq. (23), the following formula can be obtained as follows,

$$\dot{V} = -2(\lambda_i - \lambda_{\text{opt}})\left\{\varepsilon\left[(\lambda_i - \lambda_{\text{opt}})/\varphi\ \right]^2 \text{sgn}(\lambda_i - \lambda_{\text{opt}}) + k(\lambda_i - \lambda_{\text{opt}})\right\}. \tag{24}$$

In Eq. (24), the ALCs are set to be positive definite. Therefore, it can be inferred as follows,

$$\begin{cases} \dot{V} \le 0, \lambda_i \le \lambda_{\text{opt}}, \\ \dot{V} \le 0, \lambda_i > \lambda_{\text{opt}}. \end{cases} \tag{25}$$

As can be seen from Eq. (25) that $\dot{V}$ is negative definite, so the proposed sliding mode controller is stable asymptotically.

4.2 Robustness Analysis

In fact, BEV is a non-linear and uncertain system. Therefore,it is necessary to perform robust analyses. In this subsection, for the errors of the motor torque and the road adhesion coefficient, the robustness of the sliding mode controller is analyzed.

4.2.1 Motor Torque Error

There is an error between the actual output torque and the required value. Assuming that ΔT_i is the torque error, the actual torque is as follows,

$$T_{ia} = T_i + \Delta T_i, \tag{26}$$

where T_{ia} is the real output torque.

Substituting Eq. (11) into Eq. (23), the following formula can be obtained as follows,

$$\dot{V} = 2\left(\lambda_i - \lambda_{\text{opt}}\right)\left[\frac{T_i \nu}{J_i r \omega_i^2} - \mu_{\lambda i}\left(\frac{F_{zi}\nu}{J_i\omega_i^2} + \frac{F_{zi}}{rM\omega_i}\right)\right]. \tag{27}$$

Replacing T_{ia} by Eq. (26),

$$\dot{V} = 2\left(\lambda_i - \lambda_{\text{opt}}\right)\left[\frac{\Delta T_i \nu}{J_i r \omega_i^2} + \frac{T_i \nu}{J_i r \omega_i^2} - \mu_{\lambda i}\left(\frac{F_{zi}\nu}{J_i\omega_i^2} + \frac{F_{zi}}{rM\omega_i}\right)\right]. \tag{28}$$

Substituting Eq. (11) and Eq. (16) into Eq. (28),

$$\dot{V} = 2\left(\lambda_i - \lambda_{\text{opt}}\right)\left\{\frac{\Delta T_i \nu}{J_i r {\omega_i}^2} + \left\{\varepsilon\left[\left(\lambda_i - \lambda_{\text{opt}}\right)/\varphi\right]^2 \text{sgn}(\lambda_i - \lambda_{\text{opt}}) + k(\lambda_i - \lambda_{\text{opt}})\right\}\right\}. \tag{29}$$

It can be concluded that ΔT_i should satisfy the following equation,

$$|\Delta T_i| \le \left|\frac{J_i r \omega_i^2}{\nu}\left[-\varepsilon(S/\varphi\ )^2 \text{sgn}(S) - kS\right]\right|. \tag{30}$$

Lyapunov function $\dot{V}$ is less than 0 and it means that when the torque error of the driving motor satisfies Eq. (30), the sliding mode controller is stable and robust, and vice versa.

4.2.2 Adhesion Coefficient Error

The road surface adhesion coefficient is usually obtained by some estimation methods. It will lead to an error between the actual adhesion coefficient and the estimating one. $\Delta\mu_i$ is assumed as the adhesion coefficient error. Therefore, the actual adhesion coefficient μ_{ia} can be defined as follows,

$$\mu_{ia} = \Delta\mu_i + \mu_i, \tag{31}$$

Substituting Eq. (31) for μ_i in Eq. (27),

$$\dot{V} = 2\left(\lambda_i - \lambda_{\text{opt}}\right)\left[\frac{T_i \nu}{J_i r \omega_i^2} - (\Delta\mu_i + \mu_i)\left(\frac{F_{zi}\nu}{J_i\omega_i^2} + \frac{F_{zi}}{rM\omega_i}\right)\right]. \tag{32}$$

Substituting Eq. (11) and Eq. (16) into Eq. (32),

$$\dot{V} = 2(\lambda_i - \lambda_{\text{opt}})\left\{\Delta\mu_{\lambda i}\left(\frac{F_{zi}v}{J_i{\omega_i}^2} + \frac{F_{zi}}{rM\omega_i}\right) + \left\{\varepsilon\left[(\lambda_i - \lambda_{\text{opt}})/\varphi\right]^2 \text{sgn}(\lambda_i - \lambda_{\text{opt}}) + k(\lambda_i - \lambda_{\text{opt}})\right\}\right\}. \tag{33}$$

Therefore, it can be inferred that $\Delta\mu_i$ should satisfy the following equation,

$$|\Delta\mu_{\lambda i}| \le \left|\frac{J_i r\omega_i^2 M}{F_{zi}(rMv + J_i\omega)}\left[-\varepsilon(S/\varphi\ )^2\text{sgn}(S) - kS\right]\right|. \tag{34}$$

Lyapunov function $\dot{V}$ is less than 0 and it means that when the adhesion coefficient error satisfies Eq. (34), the ASR controller is stable and robust, and vice versa.

5 Vehicle Road Test

Some real vehicle tests under the two typical kinds of road conditions, wet and dry, are performed in this section to verify the performance of the proposed acceleration slip control approach. Figure 6 shows the used battery electric vehicle test platform with VCU and ABS. The ASR controller model is embedded into the VCU as a subsystem of the main functions.

A part of parameters of the used BEV are shown in Table 3. The ABS is equipped with wheel speed sensors and the signal frequency of sampling is 100 Hz. Computer sampling results have a high frequency of 1000 Hz. The used parameters of the proposed controller are listed in Table 4.

5.1 Wet Road Condition

In this subsection, the real vehicle tests are carried out on a low adhesion road condition, which is a slippery pavement with a maximum adhesion coefficient of 0.4 and an optimal slip ratio of 0.11. Because of the limited length of the road on the test site, the maximum vehicle speed should not exceed 60 km/h to reserve a sufficient safety distance.

Figure 6 Test platform of battery electric vehicle

It can be seen from Figure 7(a) and (b) that, in the absence of ASR system, the output torque of the DCS increases to the maximum value quickly and then decreases to the rated torque with the increasing speed. The slip ratio increases to about 0.7 and remains at a high level for a while. However, with the ASR system, the VCU is in the DCS by default. When the driver presses the accelerator pedal, the slip ratio and the vehicle speed exceed their thresholds respectively and the VCU enters the ASR controller. Low ABS sensor accuracy is difficult to obtain an accurate slip rate during low vehicle speed. Therefore, the BEV is accelerated to a certain speed before testing first. For the same reason, the slip ratio may approach 1 at low speed as illustrated in Figure 7(b). With the torque adjustment, the slip ratio is changing up and down along the optimal slip ratio all the time. When the vehicle speed is close to 60 km/h, the driver releases the accelerator pedal gradually and the VCU enters the DCS.

As indicated in Figure 7(c), when with the ASR system, the wheel speed is higher than vehicle speed slightly throughout the acceleration process. After 6.5 s, the vehicle speed reaches 52 km/h. The acceleration curves, shown in Figure 7(d) illustrated that, compared to the

Table 3 Parameters of the used battery electric vehicle

Description	Value
Gross vehicle weight (kg)	2200
Radius of tire (mm)	364
Wheelbase (mm)	3360
Moment of inertial of wheel (kg·m^2)	1
Transmission ratio	13.52
Unsprung mass of front axle (kg)	400
Unsprung mass of rear axle (kg)	500

Table 4 Parameters of the controller in vehicle tests

Description	Wet road	Dry road
Speed threshold v_{th} (km/h)	5.0	1.5
Optimal slip ratio λ_{th}	0.11	0.17
Slip ratio threshold λ_{opt}	0.11	0.17
Slip ratio difference λ_{dif}	0.5	0.05
Torque coefficient threshold σ	0.6	0.8
Maximum road adhesion μ_{max}	0.4	0.8
Boundary layer thickness φ	0.01	0.01

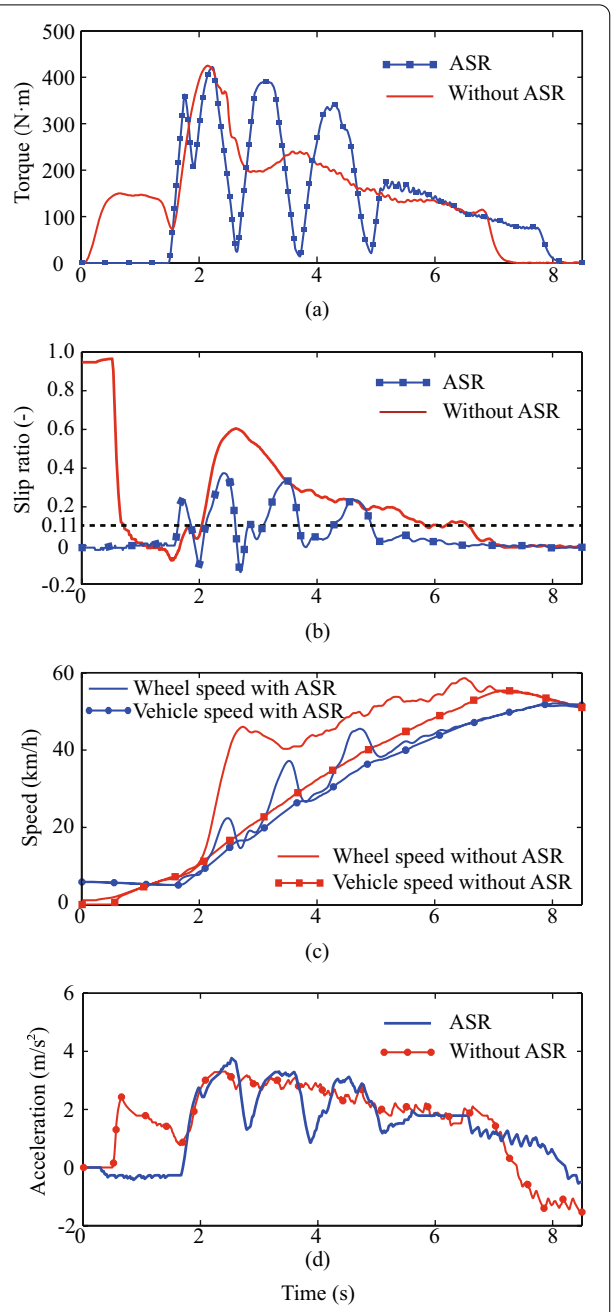

Figure 7 Vehicle test under wet road condition

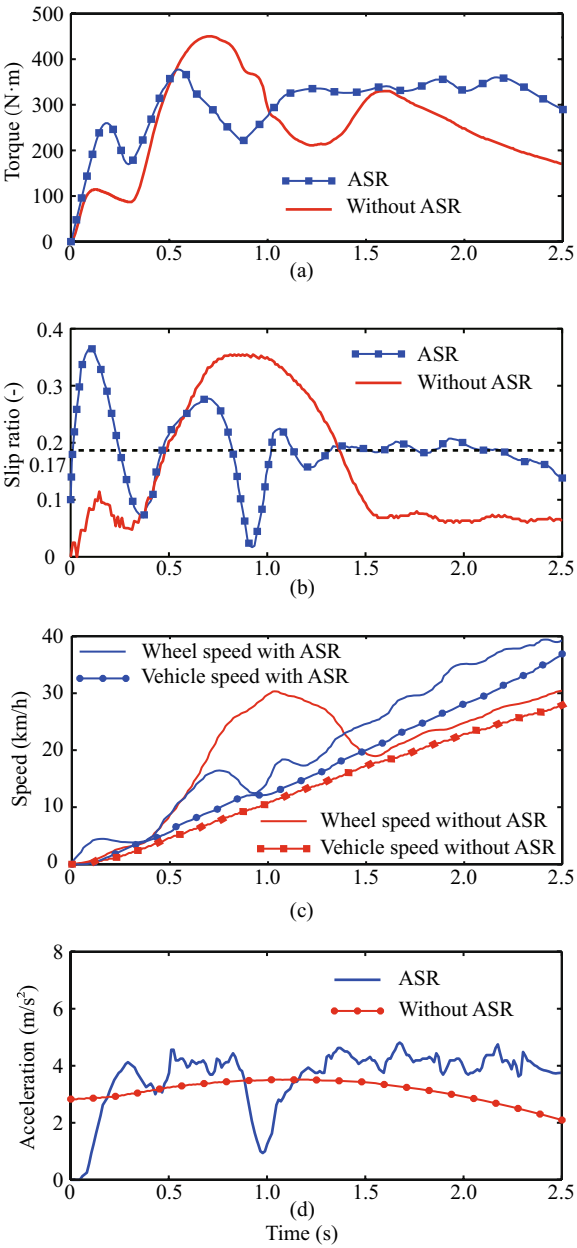

Figure 8 Vehicle test underdry road condition

DCS, it has better continuous acceleration performance. In addition, the vehicle does not show a tendency to side-slip and the vehicle posture is stable.

5.2 Dry Road Condition

In this subsection, the road condition is a dry cement pavement with a maximum adhesion coefficient of 0.8 and an optimal slip ratio of 0.17. In order to reserve a sufficient safety distance, the maximum speed does not exceed 40 km/h. It can be seen from Figure 8(a) and (b) that, in the absence of ASR system, the output torque of the DCS increases to the maximum value quickly and then decreases to the rated torque with the increasing speed. The slip ratio increases to about 0.35 and remains at a high level for a while. However, when the ASR system works, the VCU is in the DCS by default. When the driver presses the accelerator pedal, the slip ratio and the

vehicle speed exceed their thresholds respectively and the VCU enters the working mode of the ASR controller. After an adjustment process, the slip ratio stabilizes in optimal control zone and lasts about 1 s. When the vehicle speed is close to 40 km/h, the driver releases the accelerator pedal gradually and the VCU enters the DCS.

As indicated in Figure 8(c), the wheel speed is higher than the vehicle speed slightly throughout the acceleration process when with the ASR system. After 2.5 s, the vehicle speed reaches 37 km/h. The acceleration curves are shown in Figure 8(d). Compared to the DCS, the acceleration performance of BEV calculated by the mean accelerations can be improved. In addition, the vehicle does not show a tendency to side-slip and the vehicle posture is stable.

Based on the analysis above, it can be concluded that under the driving conditions of low and high adhesion roads, the proposed ASR controller can reduce the wheel slip effectively. Besides, there is good straight-line driving stability during the acceleration process. The slip ratio can be regulated around the optimal control zone and the quick response is proved.

5.3 Test Results Comparison

There are few real vehicle verifications in the field of research on the acceleration slip regulation of BEV currently. In order to further verify the control effect of the proposed approach, Ref. [14] with fuzzy control and Ref. [8] with predictive control algorithm are selected to be compared, both of which only carried out simulation validation. When the vehicle starts under slippery road, the vehicle acceleration in Ref. [14] is 1.11 m/s^2, in Ref. [8] is 2.78 m/s^2, and around 2.01 m/s^2 in this paper. It indicates that the accelerated start performance can be effectively guaranteed by the proposed approach.

As for the control effect on the wheel slip ratio, there are many uncertain interference factors in the real vehicle tests of this paper, which are not considered in the simulation validations as shown in the two comparative literatures. Although the unstable fluctuation of slip ratio is unavoidable, the tracking error of the slip ratio can be kept within a small range. Therefore, it can be concluded that the proposed approach has good control effect on the wheel slip during acceleration with high feasibility in the controller hardware.

6 Conclusions

The slip process occurs in a short period of time, which requires the ASR system to have a small overshoot and quick response. Some concluding remarks of this paper are concluded as follows.

(1) Propose a sliding mode control law to prevent the driving wheels slip by regulating the slip ratio, which provides a new idea for solving the wheel slip problem in the driving process of battery electric vehicle.
(2) Design a control algorithm on the basis of fuzzy controller to adjust key parameters of the approach law for weakening the system oscillation.
(3) Validate the effectiveness of the proposed control approach by real vehicle tests, which provides the foundation for engineering application.

The experimental results indicate that the designed control approach for the acceleration slip regulation has a small overshoot and a quick response under both low and high adhesion road conditions.

Acknowledgements
The authors sincerely thank JAC Motors, Hefei 230009, China.

Author Contributions
QS wrote and modified the manuscript; MW wrote the manuscript and carried out experiments; ZH modified the manuscript and assisted with validation; CY assisted with the experiments; YW assisted with the validation; LH was in charge of the whole research and modified the manuscript. All authors read and approved the final manuscript.

Authors' Information
Qin Shi, born in 1963, is currently a professor at *School of Automotive and Transportation Engineering, Hefei University of Technology, China*. She received her Ph.D. degree from *Hefei University of Technology, China*, in 2006. Her research interests include energy management of vehicle-road cooperative intelligent network electric vehicle, and intelligent transportation. E-mail: shiqin@hfut.edu.cn.
Mingwei Wang, born in 1995, is currently a PhD candidate at *School of Automotive and Transportation Engineering, Hefei University of Technology, China*. He received his master degree from *School of Automotive and Transportation Engineering, Hefei University of Technology, China*, in 2021. His research interests include automobile powertrain, vehicle dynamics and control, brake-by-wire system design and control, driving motor and motor control unit. E-mail: wangmingwei@mail.hfut.edu.cn.
Zejia He, born in 1997, is currently a PhD candidate at *School of Automotive and Transportation Engineering, Hefei University of Technology, China*. She received her bachelor degree in vehicle engineering from *Nanjing Agricultural University, China*, in 2019. Her research interests include vehicle system dynamics and control, design and development of vehicle electronic control system, driving energy consumption optimization, and regenerative anti-lock braking control. E-mail: hezejia@mail.hfut.edu.cn.
Cheng Yao, born in 1995, received his master degree in vehicle engineering from *School of Automotive and Transportation Engineering, Hefei University of Technology, China*, in 2021. His research interests include automobile powertrain, vehicle dynamics and control, development of vehicle electronic control system. E-mail: yaocheng950116@163.com.
Yujiang Wei, born in 1994, is currently a PhD candidate at *School of Automotive and Transportation Engineering, Hefei University of Technology, China*. He received his master degree in vehicle engineering from *Hefei University of Technology, China*, in 2020. His research interests include design and development of vehicle electronic control system, power battery design and battery management system, and driving electric motor and motor control unit. E-mail: weiyujiang@mail.hfut.edu.cn.
Lin He, born in 1977, is currently a professor at *School of Automotive and Transportation Engineering, Hefei University of Technology, China*. He received his Ph.D. degree from *Tongji University, China*, in 2010. His research interests include vehicle dynamics and control, automotive powertrain and control, and development of new energy vehicle. E-mail: helin@hfut.edu.cn.

Funding
Supported by Key Research and Development Program of Jiangsu Province of China (Grant No. BE2021006-2), University Synergy Innovation Program of Anhui Province of China (Grant No. GXXT-2020-076), Innovation Project of New Energy Vehicle and Intelligent Connected Vehicle of Anhui Province of China, and Foundation of State Key Laboratory of Automotive Simulation and Control of China (Grant No. 20201107).

Competing Interests
The authors declare no competing financial interests.

Author Details
[1]School of Automotive and Transportation Engineering, Hefei University of Technology, Hefei 230009, China. [2]Laboratory of Automotive Intelligence and Electrification, Hefei University of Technology, Hefei 230009, China.

Received: 12 December 2020 Revised: 2 March 2022 Accepted: 12 April 2022
Published online: 11 June 2022

References

[1] H W Zhang. Technical progress and development trend of electric vehicles. *International Conference on Innovations in Economic Management & Social Science*, 2017.
[2] H W He, X J Yu, F C Sun, et al. Study on power performance of traction motor system for electric vehicle. *Proceedings of the Chinese Society of Electrical Engineering*, 2006, 26 (6): 136-140.
[3] A D Yin, J Sun, H Zhao, et al. Control patterns of the automobile anti-slip regulation system and key technologies. *Journal of Hefei University of Technology (Natural Science)*, 2004, 27 (3): 325-329.
[4] H Chen, X Gong, Y F Hu, et al. Automotive control: the state of the art and perspective. *Acta Automatica Sinica*, 2013, 39 (4): 322-346.
[5] H T Peng, Z W He, H K Yu. Development analysis on permanent magnet synchronous motor in electric vehicle. *Micro Motors*, 2010, 43 (6): 78-81.
[6] Z He, Q Shi, Y Wei, et al. A model predictive control approach with slip ratio estimation for electric motor anti-lock braking of battery electric vehicle. *IEEE Transactions on Industrial Electronics*, 2021.
[7] C Zhang, G Yin, N Chen. The acceleration slip regulation control for two-wheel independent driving electric vehicle based on dynamic torque distribution. *2016 35th Chinese Control Conference (CCC)*, 2016: 5925-5930.
[8] L Yuan, H Zhao, H Chen, et al. Nonlinear MPC-based slip control for electric vehicles with vehicle safety constraints. *Mechatronics*, 2016, 38: 1-15.
[9] L I Yong, X U Xing, X Sun, et al. Review and future development of in-wheel motor drive technology. *Electric Machines & Control Application*, 2017, 44 (6): 1-718.
[10] Z Wang, X Ding, L Zhang. Overview on key technologies of acceleration slip regulation for four-wheel-independently-actuated electric vehicles. *Journal of Mechanical Engineering*, 2019, 55 (12): 99-120.
[11] L Guo, H Xu, J Zou. Acceleration slip regulation control strategy for four-wheel independent drive electric vehicles. *IEEJ Transactions on Electrical and Electronic Engineering*, 2019, 14 (4): 630-639.
[12] J W Li, B J Qu. Research on acceleration slip regulation system for two wheel drive electric vehicle. *2009 International Conference on Mechatronics and Automation*, 2009: 807-811.
[13] Y P Pan, D P Huang, Z H Sun. Overview of type-2 fuzzy logic control. *Control Theory & Applications*, 2011, 28 (1): 13-23.
[14] G Yin, S Wang, X Jin. Optimal slip ratio based fuzzy control of acceleration slip regulation for four-wheel independent driving electric vehicles. *Mathematical Problems in Engineering*, 2013: 1-7.
[15] Y G Xi, D W Li, S Lin. Model predictive control-status and challenges. *Acta Automatica Sinica*, 2013, 39 (3): 222-236.
[16] Z He, Q Shi, Y Wei, et al. A torque demand model predictive control approach for driving energy optimization of battery electric vehicle. *IEEE Transactions on Vehicular Technology*, 2021, 70 (4): 3232-3242.
[17] L He, T Shen, L Yu, et al. A model-predictive-control-based torque demand control approach for parallel hybrid powertrains. *IEEE Transactions on Vehicular Technology*, 2013, 62 (3): 1041-1052.
[18] M Sekour, K Hartani, A Merah. Electric vehicle longitudinal stability control based on a new multimachine nonlinear model predictive direct torque control. *Journal of Advanced Transportation*, 2017: 1-19.
[19] L He, W Ye, Z He, et al. A combining sliding mode control approach for electric motor anti-lock braking system of battery electric vehicle. *Control Engineering Practice*, 2020, 102: 104520.
[20] X J Mu, Y Z Chen. Overview of sliding mode variable structure control. *Control Engineering of China*, 2007, S2: 1-5.
[21] L Wu, J Gou, L Wang, et al. Acceleration slip regulation strategy for distributed drive electric vehicles with independent front axle drive motors. *Energies*, 2015, 8 (5): 4043-4072.
[22] H He, J Peng, R Xiong, et al. An acceleration slip regulation strategy for four-wheel drive electric vehicles based on sliding mode control. *Energies*, 2014, 7 (6): 3748-3763.
[23] K Han, M Choi, B Lee, et al. Development of a traction control system using a special type of sliding mode controller for hybrid 4WD vehicles. *IEEE Transactions on Vehicular Technology*, 2018, 67 (1): 264-274.
[24] L Zhou, L Xiong, Z P Yu. A research on anti-slip regulation for 4WD electric vehicle with in-wheel motors. *Applied Mechanics & Materials*, 2013: 753-757.
[25] R de Castro, R E Ara´ujo, D Freitas. Wheel slip control of EVs based on sliding mode technique with conditional integrators. *IEEE Transactions on Industrial Electronics*, 2013, 60 (8): 3256-3271.
[26] Z Wang, Y Zhou, G Lee. The sliding mode control about ASR of vehicle with four independently driven in-wheel motors based on the exponent approach law. *Energy Procedia*, 2016, 88: 827-832.
[27] C Unsal, P Kachroo. Sliding mode measurement feedback control for antilock braking systems. *IEEE Transactions on Control Systems Technology*, 1999, 7 (2): 271-281.
[28] J Y Wong. Theory of ground vehicles. *Journal of Terramechanics*, 1994.
[29] J K Liu, F C Sun. Research and development on theory and algorithms of sliding mode control. *Control Theory & Applications*, 2007, 24 (3): 407-418.